On-off switching of vortex shedding and vortex-induced vibration in crossflow past a circular cylinder by locking or releasing a rotational nonlinear energy sink

Antoine B. Blanchard and Arne J. Pearlstein

Phys. Rev. Fluids **5**, 023902 — Published 20 February 2020

DOI: 10.1103/PhysRevFluids.5.023902

On/Off Switching of Vortex Shedding and Vortex-Induced Vibration in Cross-Flow past a Circular Cylinder by Locking/Releasing a Rotational Nonlinear Energy Sink

Antoine B. Blanchard
Department of Mechanical Engineering
Massachusetts Institute of Technology, Cambridge, MA 02139, USA

Arne J. Pearlstein*
Department of Mechanical Science and Engineering
University of Illinois at Urbana–Champaign, Urbana, IL 61801, USA

We show how fully-developed vortex-induced vibration (VIV) of a linearly-sprung circular cylinder can be completely suppressed (i.e., driven to zero asymptotically in time) by release of a rotational "nonlinear energy sink", consisting of a mass rotating about the axis of the cylinder and a dissipative element damping the rotational motion of the mass. (The nonlinear energy sink is located either inside the cylinder or beyond the spanwise extent of the flow, with which it thus interacts only through inertial coupling to the rectilinear motion of the cylinder.) We also show that VIV can be turned on by "locking up" the rotating mass. Once VIV is suppressed or turned on, no further action or energy input is required. Thus, this approach provides a true "switch". Applications for flow control, and for turning mixing on or off, are discussed.

* E-mail for correspondence: ajp@illinois.edu

I. INTRODUCTION

For a linearly-sprung circular cylinder in cross flow, we have recently shown that introduction of a rotational "nonlinear energy sink" (NES) consisting of a) a mass rotatable at fixed radius about the axis of the cylinder, and b) a dissipative element that damps rotational motion of that mass, can have profound effects on the flow and cylinder vibration [1, 2]. The NES is either inside the cylinder, or lies beyond the spanwise extent of the flow, and so has no direct contact with the flow, exerting its influence only through its inertial coupling to the rectilinear rigid-body motion of the cylinder. Among the results found by Tumkur *et al.* [1] and Blanchard *et al.* [2] are a) "partial stabilization" of the wake during a significant fraction of a slowly decaying chaotic cycle, during which a well-defined vortex street gives way to an elongated wake with much less unsteadiness and much lower cylinder vibration amplitude, and b) coexistence of multiple long-time solutions (including multiple unsteady two-dimensional long-time solutions) for a wide range of combinations of the Reynolds number and a dimensionless spring constant.

An important question raised by that work is whether vortex shedding and vortex-induced vibration (VIV) can be *completely* suppressed (asymptotically driven to, and maintained at, zero) in a controllable way. That would make it possible to switch off (and possibly switch on) the effects of shedding and vibration at will, as might be desired in mixing applications in low-Reynolds-number flows [3, 4].

In what follows, we show, at relatively low Reynolds numbers, that it is indeed possible to completely suppress shedding and vibration by means of a rotational NES. Specifically, by switching the rotatable mass from "locked" (so that it translates rectilinearly with the cylinder, but cannot rotate) to "unlocked" (so that it is free to rotate about the axis of the sprung cylinder), one can transition from a state of time-periodic vortex shedding and cylinder vibration to a state in which the flow is steady and the cylinder is motionless. Similarly, shedding and vibration can be turned on by locking the NES mass, which leads to a transition from steady flow and no cylinder vibration to a situation characterized by VIV and enhanced wake unsteadiness.

The remainder of the paper is organized as follows. We briefly present the formulation and computational approach in §II, followed by the results in §III, a discussion in §IV, and conclusions in §V.

II. FORMULATION AND APPROACH

A. Physical model

The physical problem is identical to that considered by Tumkur *et al.* [1] and Blanchard *et al.* [2], and is shown schematically in figure 1. A Newtonian fluid with constant density ρ_f and kinematic viscosity ν flows past a linearly-sprung circular cylinder with diameter D. The cylinder is allowed to move transversely with respect to the mean flow, restrained by a linear spring with spring constant K_{cyl} per unit length of span. The NES consists of two components. First, an attached mass is allowed to rotate about the cylinder axis. Second, a viscous damper retards the rotation of the attached mass with a torque linearly proportional to the latter's angular velocity (with coefficient C_{NES}). As discussed previously [1, 2], any distributed mass is dynamically equivalent to a point or line mass a distance r_0 from the axis, with the ratio of the distributed rotating mass to the concentrated mass depending on the radius of gyration of the distributed mass and the radial location of its center of mass.

The dimensionless equations are identical to those considered previously [1, 2], and are given by

$$\frac{\partial \mathbf{v}}{\partial \tau} + \mathbf{v}\cdot\nabla\mathbf{v} = -\nabla p + \frac{1}{Re}\nabla^2\mathbf{v}, \tag{1a}$$

$$\nabla\cdot\mathbf{v} = 0, \tag{1b}$$

$$\frac{\mathrm{d}^2 y_1}{\mathrm{d}\tau^2} + \left[2\pi\frac{g_n^*}{Re}\right]^2 y_1 = \varepsilon_p \bar{r}_0 \frac{\mathrm{d}}{\mathrm{d}\tau}\left[\frac{\mathrm{d}\theta}{\mathrm{d}\tau}\sin\theta\right] + \frac{2C_L}{\pi m^*}, \tag{2a}$$

$$\frac{\mathrm{d}^2\theta}{\mathrm{d}\tau^2} + \frac{\zeta}{Re}\frac{\mathrm{d}\theta}{\mathrm{d}\tau} = \frac{\sin\theta}{\bar{r}_0}\frac{\mathrm{d}^2 y_1}{\mathrm{d}\tau^2}, \tag{2b}$$

where velocity, time, and length (including cylinder displacement) are scaled with the cylinder diameter D and free-stream velocity U, the Reynolds number is defined by $Re = UD/\nu$, θ is the angular position of the NES mass, and C_L is the lift coefficient. We take $\theta = 0$ to coincide with the positive y-axis. As earlier [1, 2], we choose the other dimensionless parameters to be independent of U. They are a density ratio $m^* = \rho_b/\rho_f$, a dimensionless natural frequency $g_n^* = D^2\sqrt{K_{cyl}/(M_{cyl}+M_{NES})}/(2\pi\nu)$ of the linear spring (e.g., *in vacuo*), the ratio ε_p of the NES mass per unit length to the sum of the total mass per unit length of the cylinder (the nonrotatable part and the attached rotatable mass), a dimensionless radius $\bar{r}_0 = r_0/D$, and a dimensionless damping parameter $\zeta = C_{NES}D^2/(\nu r_0^2 M_{NES})$.

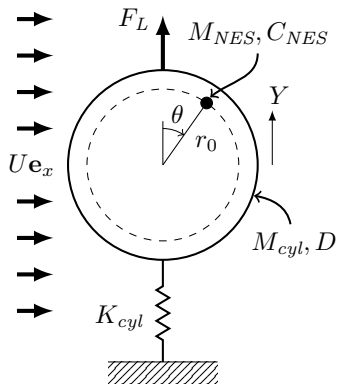

FIG. 1. Linearly-sprung cylinder in cross-flow with rotational NES.

Here, the effective density of the cylinder is $\rho_b = (M_{cyl} + M_{NES})/(\pi D^2/4)$, where M_{cyl} and M_{NES} are the masses of the nonrotatable part of the cylinder and the NES, respectively, in each case divided by the spanwise extent of the flow. We note that placing the NES beyond the span of the flow relaxes the constraints on NES design discussed by Tumkur *et al.* [1], and that placing some of the nonrotatable mass beyond the span allows high values of m^* in liquids without resorting to tungsten or other very dense metals. Compared to a more common nondimensionalization using $U^* = U\sqrt{(M_{cyl} + M_{NES})/K_{cyl}}/D = Re/(2\pi g_n^*)$, variation of U in our approach affects only Re, rather than Re and U^*.

B. Computational approach

The computational method closely follows that in our earlier work [1, 2]. We use the open-source Navier–Stokes solver Nek5000 [5] on a computational domain extending $24D$ in the cross-stream direction and $48D$ in the streamwise direction, with the undisplaced cylinder center located $12D$ away from the inlet boundary and equidistantly from the side-walls. In our production runs, the mesh consists of $n_e = 3614$ spectral elements with polynomial order $N = 5$, and the time-step size is $\Delta\tau = 10^{-3}$. The domain size, mesh topology, and time-step size are identical to those used by Tumkur *et al.* [1] and similar to those used by Blanchard *et al.* [2], and ensure adequate convergence of the results.

As in our previous work, the time-step size used is sufficiently small that no fluid-structure interaction iteration is necessary.

C. Fully-developed standard VIV

When the NES is locked, VIV occurs as if the cylinder was a single rigid body, and we refer to the long-time, time-periodic solution as fully-developed standard VIV. We compute that flow using an inlet transient asymmetric about $y = 0$,

$$\mathbf{v}_{in}(y,\tau;\alpha) = \mathbf{e}_x \begin{cases} \left[1 + \alpha e^{-(y-1)^2/2}\right]\left[1 - \dfrac{\tau}{25}\right] + \dfrac{\tau}{25}, & \text{for } 0 < \tau < 25, \\ 1, & \text{for } \tau \geq 25, \end{cases} \tag{3}$$

along with a compatible initial condition $\mathbf{v}(x,y,0) = \mathbf{v}_{in}(y,0;\alpha)$. The inlet transient becomes a uniform steady inlet condition in finite time (at $\tau = 25$), thus allowing us to "excite" VIV (with the degree of asymmetry of the imposed disturbance being governed by α). The uniform inlet flow to which the transient provides a smooth transition in finite time is consistent with VIV solutions and with a steady, symmetric, motionless-cylinder (SSMC) solution

$$v_x(x,y,\tau) = v_x(x,-y,\tau), \tag{4a}$$
$$v_y(x,y,\tau) = -v_y(x,-y,\tau), \tag{4b}$$
$$p(x,y,\tau) = p(x,-y,\tau), \tag{4c}$$

where the vorticity distribution is anti-symmetric about $y = 0$. Compared to imposing an initial condition at $\tau = 0$ in the domain and a uniform inlet condition thereafter, our approach has the advantage that there is no incompatibility

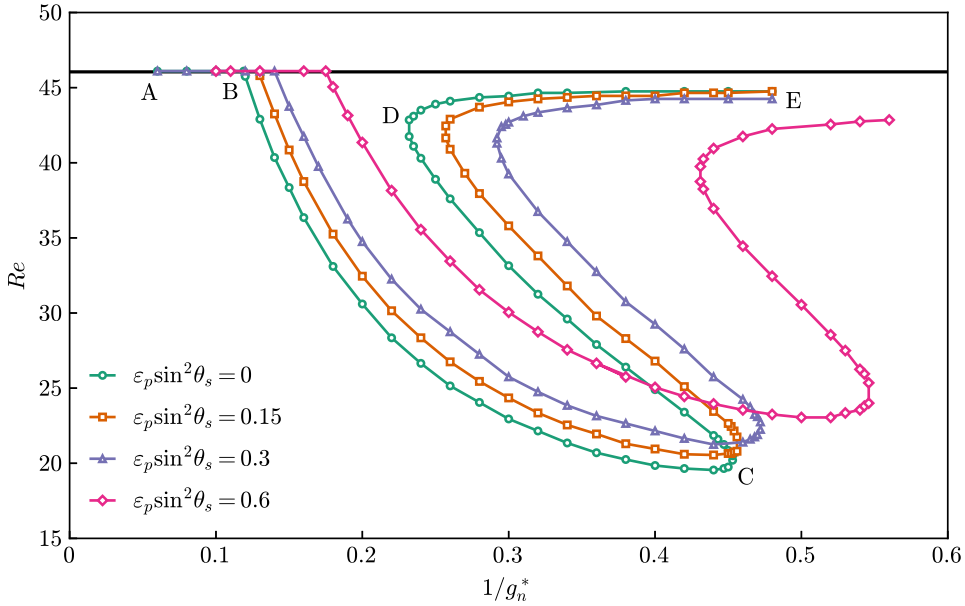

FIG. 2. Effect of a rotational NES (with $\zeta = 4/3$ and $\bar{r}_0 = 0.3$) on the stability of the steady, symmetric, motionless-cylinder solution for $\varepsilon_p \sin^2\theta_s = 0$ (green open circles), $\varepsilon_p \sin^2\theta_s = 0.15$ (orange open squares), $\varepsilon_p \sin^2\theta_s = 0.3$ (purple open triangles), and $\varepsilon_p \sin^2\theta_s = 0.6$ (pink open diamonds). The horizontal line at $Re = 46.05$ is the critical value for the fixed cylinder.

at $y = 0$, $\tau = 0$. Our approach can be thought of as a variation on the use of persistent inlet excitation [6, 7], but with a finite duration, since persistent inlet excitation would not allow an SSMC solution.

In what follows, we take $m^* = 10$. Except where otherwise stated, $\zeta = 4/3$ and $\bar{r}_0 = 0.3$.

III. RESULTS

A. Stability boundaries

To identify conditions under which NES release might completely suppress cylinder vibration and vortex shedding, we first determine conditions under which the SSMC solution is stable with an NES, and unstable without one.

For fixed values of m^*, ζ, and $\bar{r}_0$, Tumkur *et al.* [1] and Blanchard *et al.* [2] used the approach of Zielinska and Wesfreid [9] to establish a stability boundary in the Re–$1/g_n^*$ plane for NES-less and NES-equipped linearly-sprung cylinders, with the base state an SSMC solution. For the NES-equipped case, Tumkur *et al.* [1] showed analytically that the linear stability of an SSMC solution depends only on Re, $1/g_n^*$, m^*, ζ, and a combined parameter $\varepsilon_p \sin^2\theta_s$ (where θ_s is the steady NES angular position), whereas the full nonlinear dynamical response depends on Re, $1/g_n^*$, m^*, ζ, ε_p, $\bar{r}_0$, and the initial value of θ.

Figure 2 shows four stability boundaries corresponding to $\varepsilon_p \sin^2\theta_s = 0$, 0.15, 0.3, and 0.6, computed using inlet transient (3) with $\alpha = 10^{-4}$. The combined parameter $\varepsilon_p \sin^2\theta_s$ was varied by setting $\theta_s = \pi/2$ and changing ε_p accordingly. As discussed previously [1, 2], the base flow was judged to be linearly stable only if the long-time solution computed using the full nonlinear equations (1a,b) and (2a,b) was an SSMC solution with the final value of θ tending to its initial value as $\alpha \to 0$. On the other hand, situations in which the long-time solution was unsteady, or was an SSMC solution with θ differing more than infinitesimally from its initial value, were deemed linearly unstable.

For each value of $\varepsilon_p \sin^2\theta_s$, the stability boundary divides the Re–$1/g_n^*$ plane into two parts. On the side that includes $Re = 0$, the SSMC solution is stable, while on the other side it is not. Figure 2 shows that the stability boundaries for the NES-less and NES-equipped cases are qualitatively similar, being single-valued for sufficiently large and small values of $1/g_n^*$, and triple-valued in an intermediate range of $1/g_n^*$. As $\varepsilon_p \sin^2\theta_s$ increases, the stability boundary deviates more strongly from that for the NES-less case, in what appears to be a continuous deformation of the NES-less boundary. The double-Hopf point (denoted by B for the NES-less case in figure 2) shifts to larger values of $1/g_n^*$ as $\varepsilon_p \sin^2\theta_s$ increases, with $(1/g_n^*)_B$ assuming values of 0.119, 0.128, 0.140, and 0.172 for $\varepsilon_p \sin^2\theta_s = 0$, 0.15, 0.3, and 0.6, respectively. Figure 2 also shows that for increasing values of $\varepsilon_p \sin^2\theta_s$, the right turning point C moves to larger values of Re and $1/g_n^*$, while the left turning point D is displaced to larger values of $1/g_n^*$ and smaller Re. For sufficiently small $1/g_n^*$, the stability boundaries for the NES-less and NES-equipped cases coincide with the

fixed-cylinder stability boundary for all values of $\varepsilon_p \sin^2\theta_s$ considered. In the limit $1/g_n^* \to \infty$, the upper branch of the stability boundaries (denoted by D–E in the NES-less case) appears to slowly approach the fixed-cylinder stability boundary as $\varepsilon_p \sin^2\theta_s$ increases.

For each nonzero value of $\varepsilon_p \sin^2\theta_s$, there is a portion of the Re–$1/g_n^*$ plane in which the SSMC solution is linearly stable in the NES-equipped case, and is unstable with no NES. Figure 2 shows that this NES-stabilizable portion of the Re–$1/g_n^*$ plane grows with increasing $\varepsilon_p \sin^2\theta_s$, and that a large part of the region below $Re = 46.05$ (the stability boundary for a fixed cylinder) in which the NES-less case is unstable is rendered stable in the NES-equipped case for $\varepsilon_p \sin^2\theta_s = 0.6$. It is in the NES-stabilizable portion of the Re–$1/g_n^*$ plane where we investigate whether cylinder vibration and vortex shedding can be completely suppressed by release of an NES, or triggered by locking the NES.

B. Complete suppression of fully-developed vortex shedding and VIV

We begin by computing the fully-developed standard VIV solution with the NES mass locked in a fixed position, from which it will later be released. (In all that follows, the NES mass is released with zero angular velocity.) For $Re = 24$, $1/g_n^* = 0.3$, and $\varepsilon_p = 0.3$ (in the NES-stabilizable region), movie 1 [8] and the first 1500 convective time units of figures 3a-e show that when the NES is released from $\theta_{release} = \pi/2$ at $\tau = 696.46$ (well into the fully-developed standard VIV regime), there is a rather quick transition to an SSMC solution. (Figures S1a-e [8] show the first 1500 convective time units of each time series in more detail. The remainder of the time series in figures 3a-e, i.e., for $1500 \le \tau \le 4000$, is discussed in §III C.)

The physical mechanism is as follows. Immediately after the mass is released, rotation begins, with inertial coupling to the rectilinear motion of the cylinder leading to energy transfer from the cylinder to the rotating mass. In less than 50 convective time units, the NES mass rapidly swings through several multiples of 2π, dissipating a significant amount of kinetic energy from the cylinder motion, whose amplitude is reduced by nearly 85% between $\tau = 696.46$ and 741.46 (figure 3a). The NES continues to bleed off kinetic energy from the cylinder motion as the cylinder becomes asymptotically motionless. As the rectilinear motion ceases, the NES mass settles at a steady angular displacement of about $\theta_s = 9.25\pi$ (figure 3b), corresponding to an SSMC solution with $\varepsilon_p \sin^2\theta_s \approx 0.230$. Figure 2 shows that for $Re = 24$ and $1/g_n^* = 0.3$, the SSMC solution is linearly stable for $\varepsilon_p \sin^2\theta_s > 0.15$, so that this final state is a finite distance from the stability boundary.

It is useful to consider how the capability to completely suppress cylinder vibration and vortex shedding depends on the phase of cylinder vibration ($\phi_{release}$) at which NES release occurs. (Here, $\phi_{release} = 0$ and $\phi_{release} = \pi$ are the phases at which $y_1 = -A$ and $y_1 = A$, respectively, where A is the amplitude of cylinder vibration.) For $\theta_{release} = (2n+1)\pi/2$ (n an integer), it is sufficient to investigate values of $\phi_{release}$ in the range $[0, \pi)$ because of symmetry. (Details are shown in the Supplemental Material [8].) For $\theta_{release} \neq (2n+1)\pi/2$, one must consider the full range $[0, 2\pi)$ of $\phi_{release}$.

Table I shows results for 35 values of $0 \le \phi_{release} < \pi$, with the largest gap between values being 0.05. For the values investigated, complete suppression was found in three subranges. (No attempt was made to systematically delineate the subranges of $\phi_{release}$ in which complete suppression can be achieved, and so there might be more.) In each such subrange, $\varepsilon_p \sin^2\theta_s$ exceeds 0.116 ± 0.001, the critical value that we compute for $Re = 24$ and $1/g_n^* = 0.3$. We can interpret the release phase $\phi_{release}$ as specifying an initial condition (with velocity and pressure fields, and a cylinder position and velocity) for the evolution of the NES-equipped case beginning at the release time. In this one-parameter subspace of the initial condition space, table I suggests that the subranges in which complete suppression occurs are continuous, rather than fractal or riddled [10].

For values of $\phi_{release}$ for which suppression is not achieved, release of the NES is immediately followed by a large reduction in rectilinear amplitude, followed by an interval of slow growth. This eventually leads to a quasi-periodic long-time solution with rms displacement of 0.1045 ± 0.0005, slightly less than that for NES-less fully-developed standard VIV (0.1934), and with significant rotation of the NES mass. (See figure 4a-e for $0 \le \tau \le 2000$, movie 2 [8], and figures S2a-e and S3 [8] for release from $\theta_{release} = \pi/2$ and at $\tau = 698.57$, which corresponds to $\phi_{release} = 0.65\pi$.) These solutions (for $0 \le \tau \le 2000$) correspond to the quasi-periodic solutions found by Blanchard *et al.* [2] for $Re = 24$ and $1/g_n^* = 0.3$ using a rotational NES that is unlocked beginning at $\tau = 0$.

To characterize performance in cases for which cylinder vibration is completely suppressed, we define $\tau_{0.01}$ as the elapsed time between release of the NES mass and the last time that the maximum cylinder excursion exceeds 1% of the pre-release amplitude. (We do not use an exponential decay rate, because the process is initially significantly nonlinear.) Table I shows that when suppression occurs, $\tau_{0.01}$ depends strongly on the phase of the cylinder motion at which the NES is released, with a more than two-fold difference between the smallest (146.89) and largest (298.19) values of $\tau_{0.01}$. Dispersion in $\tau_{0.01}$ values is due to failure of this measure to account for the regime transition that occurs in the suppression process. Figure 5 shows that release of the NES is followed by an interval during which the amplitude of y_1 decays nonexponentially, with strongly nonlinear dynamics. After just a few time units, oscillations

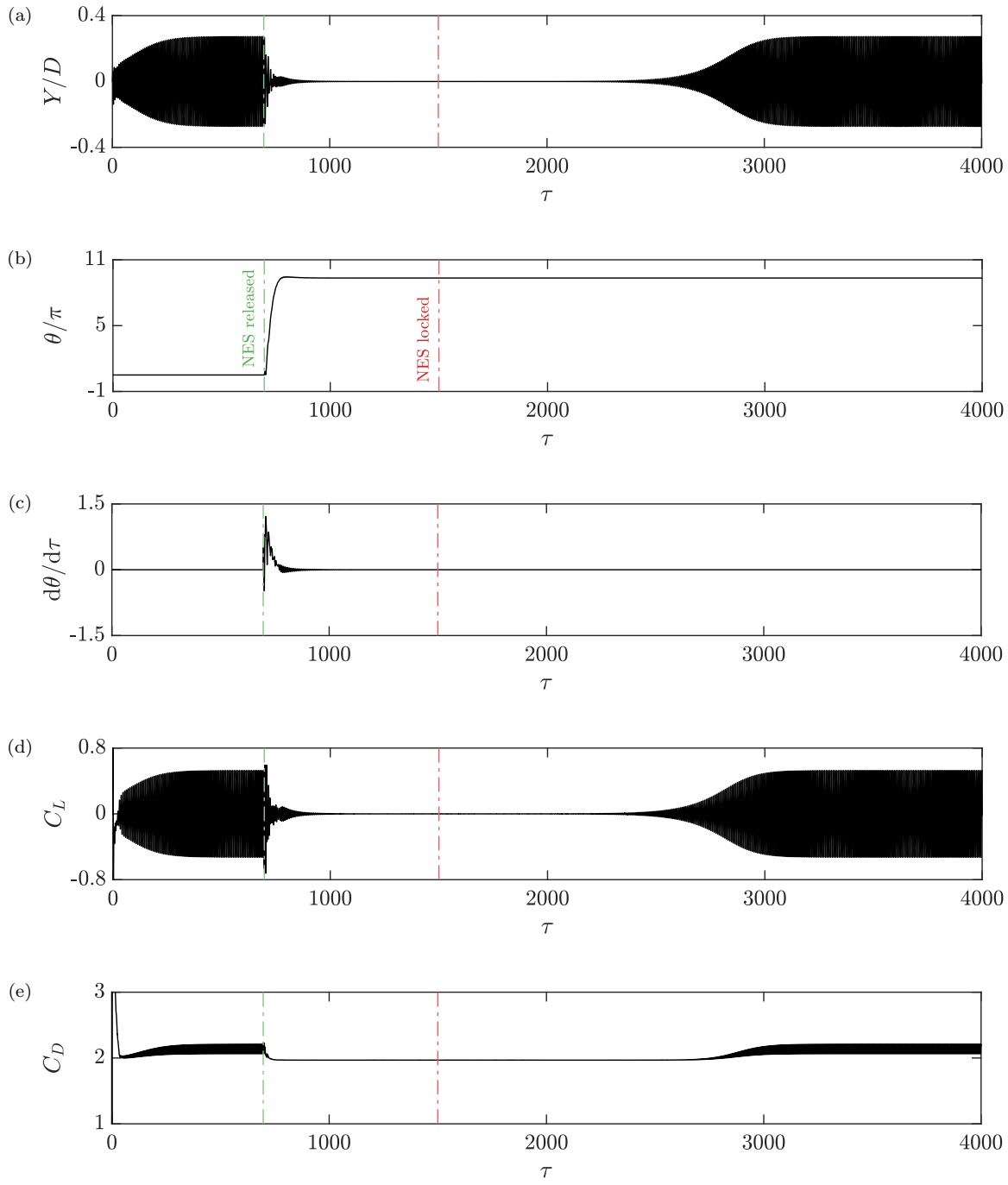

FIG. 3. Time series for $Re = 24$ and $1/g_n^* = 0.3$, where a rotational NES with $\varepsilon_p = 0.3$ is released from $\theta_{release} = \pi/2$ at $\tau = 696.46$ (corresponding to $\phi_{release} = 0.113\pi$), and locked at $\tau = 1500$: (a) cylinder displacement, (b) NES angular displacement, (c) NES angular velocity, (d) lift coefficient, and (e) drag coefficient.

in y_1 have become so small that nonlinear effects are no longer significant, and the dynamics are approximately linear. From this point forward, the decay in y_1 is exponential (figure 5), with decay rate depending significantly on $\varepsilon_p \sin^2 \theta_s$.

This transition from nonexponential to exponential decay calls for another measure of performance. We define τ_{nl} as the elapsed time between release of the NES mass and the beginning of exponential decay, determined as follows. Over each of a series of overlapping time intervals $[\tau_i, \tau_i + 60]$, we fit the model

$$y_{fit}(\tau) = A_i \exp[-a_i(\tau - \tau_i)] \tag{5}$$

to the local maxima of $y_1(\tau)$, with τ_i ranging from 600 (nearly 100 time units before NES release) to 1200 (well into

$\tau_{release}$	$\phi_{release}/\pi$	Long-time solution	$\varepsilon_p \sin^2\theta_s$	$\tau_{0.01}$	τ_{nl}
696.016	0.000	Quasi-periodic	–	–	–
696.212	0.050	Quasi-periodic	–	–	–
696.408	0.100	Quasi-periodic	–	–	–
696.456	0.112	SSMC	0.271	218.11	111.54
696.460	0.113	SSMC	0.230	249.03	125.54
696.486	0.120	Quasi-periodic	–	–	–
696.508	0.125	Quasi-periodic	–	–	–
696.604	0.150	Quasi-periodic	–	–	–
696.802	0.200	Quasi-periodic	–	–	–
696.998	0.250	Quasi-periodic	–	–	–
697.194	0.300	Quasi-periodic	–	–	–
697.390	0.350	Quasi-periodic	–	–	–
697.442	0.363	Quasi-periodic	–	–	–
697.490	0.375	Quasi-periodic	–	–	–
697.588	0.400	SSMC	0.223	230.17	100.41
697.784	0.450	SSMC	0.275	154.09	88.22
697.948	0.492	SSMC	0.233	146.92	102.06
697.980	0.500	SSMC	0.232	146.89	102.02
698.176	0.550	SSMC	0.273	153.71	87.82
698.374	0.600	SSMC	0.265	191.44	103.63
698.422	0.612	SSMC	0.169	298.19	105.58
698.472	0.625	Quasi-periodic	–	–	–
698.570	0.650	Quasi-periodic	–	–	–
698.598	0.657	Quasi-periodic	–	–	–
698.726	0.690	Quasi-periodic	–	–	–
698.766	0.700	SSMC	0.200	229.48	111.23
698.806	0.710	SSMC	0.298	184.04	89.19
698.844	0.720	Quasi-periodic	–	–	–
698.962	0.750	Quasi-periodic	–	–	–
699.160	0.800	Quasi-periodic	–	–	–
699.356	0.850	Quasi-periodic	–	–	–
699.454	0.875	Quasi-periodic	–	–	–
699.552	0.900	Quasi-periodic	–	–	–
699.600	0.912	Quasi-periodic	–	–	–
699.748	0.950	Quasi-periodic	–	–	–

TABLE I. For $Re = 24$ and $1/g_n^* = 0.3$, performance of a rotational NES (with $\varepsilon_p = 0.3$) released from $\theta_{release} = \pi/2$ as a function of the phase of cylinder motion at which release occurs ($\phi_{release}$).

the asymptotic regime) in increments of two. In intervals during which decay of y_1 is clearly exponential, the interval contains about ten maxima of y_1. For each interval, we assess goodness of the fit (5) by computing the residual measure $\|y_{fit}(\tau_k) - y_1(\tau_k)\|_2/A$, where τ_k corresponds to a local maximum of y_1 in the interval. The residual should be small in intervals of exponential decay, and large in intervals of strongly nonlinear behavior. We take τ_{nl} to be the largest value of τ_i for which the residual exceeds 0.05. With this measure, the NES performance is based solely on how quickly the NES suppresses nonlinear effects. In contrast to $\tau_{0.01}$, the quantity τ_{nl} is not affected by the exponential rate of approach to the SSMC solution, which depends on Re, $1/g_n^*$ and $\varepsilon_p \sin^2\theta_s$. Table I shows that there is less variability in τ_{nl} than in $\tau_{0.01}$, suggesting that when suppression occurs, nonlinear reduction of VIV amplitude by energy transfer to the rotating mass, followed by dissipation, is approximately independent of $\phi_{release}$.

The combination of density ratio ($m^* = 10$) and NES parameters ($\zeta = 4/3$, $\bar{r}_0 = 0.3$, and $\varepsilon_p \sin^2\theta_{release} = 0.3$) considered above is one for which we have already determined a stability boundary (figure 2). But there is nothing unique about these values, or the values of $1/g_n^*$ (0.3) and Re (24) considered. Indeed, the approach should work for any combination of m^*, ζ, $\bar{r}_0$, ε_p, and $1/g_n^*$ for which there is a range of Re between the lower branches of the stability boundaries for the NES-less case ($\varepsilon_p = 0$, corresponding to the green open circles in figure 2) and an NES-equipped case ($\varepsilon_p \sin^2\theta_{release} > 0$). This is supported by the results shown in figure S4a-e [8] ($m^* = 10$, $\zeta = 1$, $\bar{r}_0 = 0.25$, $\varepsilon_p = 0.4$, and $\theta_{release} = \pi/2$), a case for which we have no stability boundary, and where complete suppression is achieved with $1/g_n^* = 0.2$ and $Re = 35$, using $\phi_{release} = \pi/4$. With the indicated choices of m^*, ζ, $\bar{r}_0$, ε_p, and $1/g_n^*$, only three trial simulations were required to identify a Reynolds number and release phase leading to complete suppression.

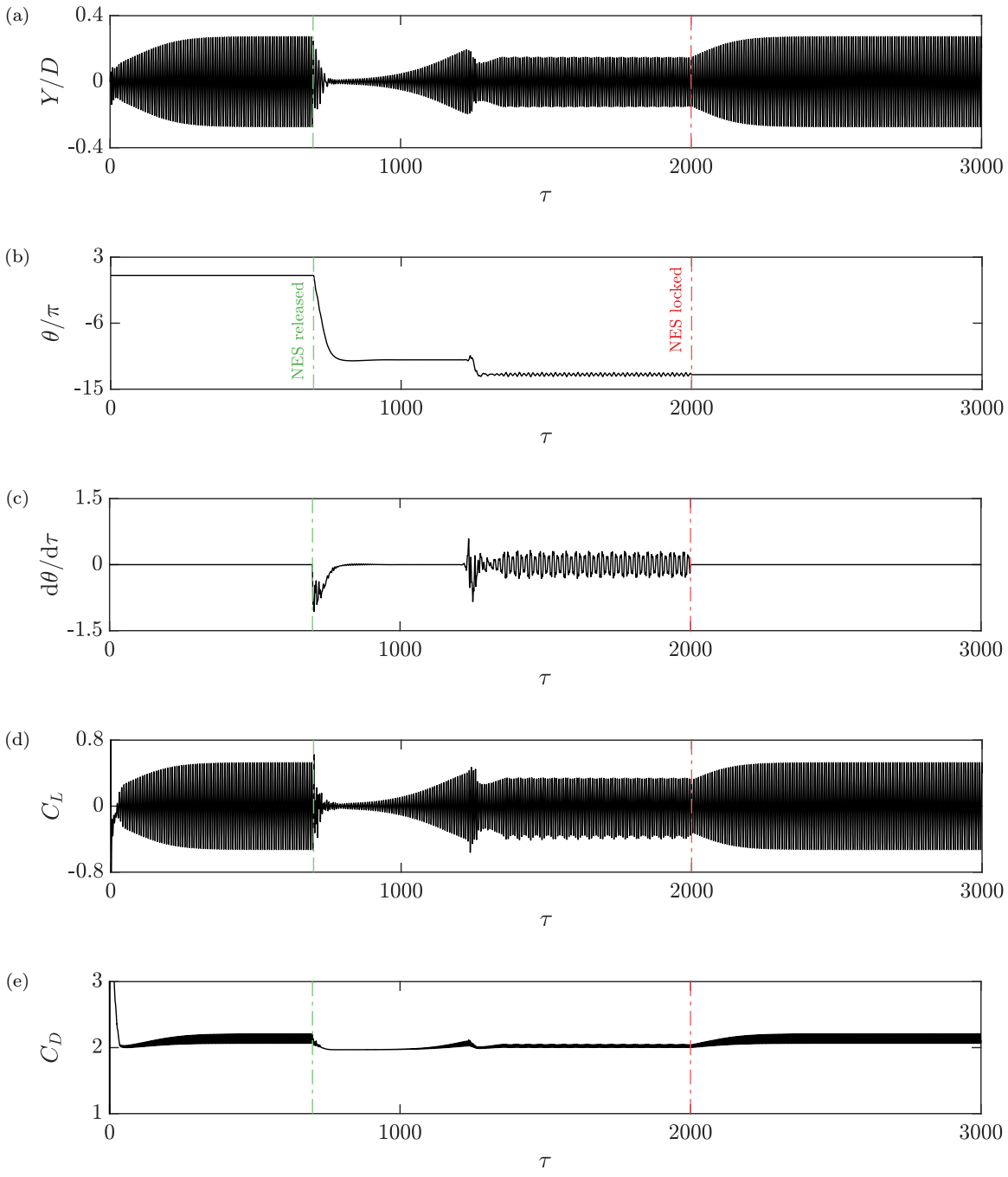

FIG. 4. Time series for $Re = 24$ and $1/g_n^* = 0.3$, where a rotational NES with $\varepsilon_p = 0.3$ is released from $\theta_{release} = \pi/2$ at $\tau = 698.57$ (corresponding to $\phi_{release} = 0.65\pi$), and locked at $\tau = 2000$: (a) cylinder displacement, (b) NES angular displacement, (c) NES angular velocity, (d) lift coefficient, and (e) drag coefficient.

C. Switching on vortex shedding and VIV

It can also be shown that for any combination of Re and $1/g_n^*$ in the NES-stabilizable range, cylinder vibration and vortex shedding can be switched on after an SSMC solution has been reached. This is done by locking the NES rotating mass, which is tantamount to turning off inertial coupling between NES rotational motion and cylinder motion in (2a,b). (When the NES mass is locked, its angular position is constant and its angular velocity is zero for all times.)

For $Re = 24$, $1/g_n^* = 0.3$, and $\varepsilon_p = 0.3$ (the same combination of parameters for which complete suppression was demonstrated in §III B), figures 3a-e show that release of the NES from $\theta_{release} = \pi/2$ at $\tau = 696.46$ leads to

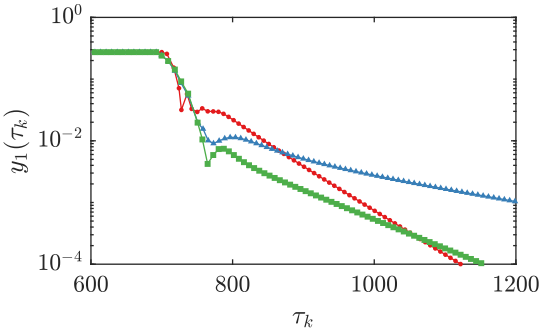

FIG. 5. Time series for maxima of cylinder displacement for $Re = 24$, $1/g_n^* = 0.3$, $\varepsilon_p = 0.3$, $\theta_{release} = \pi/2$, and $\phi_{release} = 0.112\pi$ (red circles), $\phi_{release} = 0.5\pi$ (green squares), and $\phi_{release} = 0.612\pi$ (blue triangles). Each symbol corresponds to a maximum of y_1. The lines connecting consecutive symbols merely facilitate visualization, and should not be thought of as the result of interpolation between data points.

complete VIV suppression, and ultimately to an SSMC state, as discussed in §III B. By $\tau = 1500$, the magnitudes of the cylinder displacement, NES angular velocity, and lift coefficient have decreased to below 10^{-5}, 10^{-5}, and 10^{-4}, respectively. At that time, the NES mass is locked, and remains locked thereafter. Locking the NES mass has the effect of severing inertial coupling between NES rotation and cylinder motion, as for the $\varepsilon_p = 0$ case. As the combination $(Re, 1/g_n^*) = (24, 0.3)$ lies on the unstable side of the NES-less stability boundary (figure 2), a linear instability sets in, and the trajectory at long times settles into a fully-developed standard VIV solution (figures 3a-e). This shows that in the NES-stabilizable part of the Re–$1/g_n^*$ plane, where the SSMC solution is unstable for the NES-less case, it is possible to switch on VIV at will by locking the NES, so that it has no dynamical effect on the cylinder motion and the flow.

IV. DISCUSSION

While it is clear that linear stability of the SSMC solution depends on $\varepsilon_p \sin^2\theta_s$, but not on $\bar{r}_0$ or independently on ε_p or θ_s, it is not clear how suppression of cylinder vibration and vortex shedding depends on $\bar{r}_0$, ε_p or $\theta_{release}$. Even if one were to perform a Floquet analysis of the fully-developed (time-periodic) standard VIV solution, that would reveal only information about its linear stability, and not about the long-term solution to which it will evolve if unstable. The dependence of VIV suppression on these parameters and $\phi_{release}$ can be investigated computationally, with expectations about the experimental realizability of the long-time solutions being similar to those discussed by Blanchard *et al.* [2].

From a practical standpoint, it is relatively simple to release the rotating mass at a prescribed time, or even at a prescribed phase in the cylinder motion, either using an electromagnet, or mechanically. On the other hand, locking the rotating mass instantaneously (as we have in §III C) is an idealization, because its angular velocity cannot be made zero instantaneously. The rotating mass can be brought to rest by a frictional torque larger than the term on the right-hand side of (2b), by a magnetic torque, or by mechanical "stops" that "pop up" (inside the cylinder, or beyond the spanwise extent of the flow) at azimuthal positions bracketing the current angular position of the rotating mass, which they then approach from each side. Fortunately, in the locked case (equivalent to an NES-less cylinder), the fully-developed standard VIV solution appears to be globally attracting in this part of the parameter space [11], so that there is good reason to believe that switching on cylinder vibration by locking the rotating mass should not depend on how the latter is decelerated.

If in an experiment or application it is not possible to sense the phase of cylinder vibration and to time the release of the rotatable mass accordingly, then one can pursue the following strategy. First, release the rotatable mass at some arbitrary phase. If suppression is not achieved within a reasonable time, judgable by, say, τ_{nl}, then the mass can be re-locked (at $\tau = 2000$ in figures 4a-e), with the expectation that the resulting quasi-periodic (or temporally more complex [2]) flow will revert to fully-developed standard VIV, as shown in figures 4a-e for $2000 \leq \tau \leq 3000$. The release can then be repeated, and if suppression is not achieved, the rotating mass can be locked again and the process repeated until successful. Provided that at least one subrange of $\phi_{release}$ for which complete suppression occurs has nonzero width, this approach will ultimately succeed.

The ability to release or lock a rotatable mass (e.g., using an electromagnet) provides a way to switch off or switch on flow-induced vibration in a cross-flow at low Re. As such, it enhances the potential to use flow-induced vibration to promote thermal mixing, or chemical mixing and reaction [3, 4]. We note that once the rotatable mass is released

or locked, no further actuation or energy input is required. Thus, this approach provides a true switch.

While the complete suppression described above is possible only between the lower branches of the stability boundaries for an NES-equipped and NES-less cylinder (and hence below the fixed-cylinder stability boundary just below $Re = 50$), it is clear from our earlier work [1] that a rotational NES can significantly reduce the amplitude of VIV at higher Re. Because turning on or off the rotational NES does not move a stability boundary across the "operating point" in the Re–$1/g_n^*$ plane, it is not clear whether there will be any effect of the "release phase" or "locking phase", as there is at lower Re.

From a switching standpoint, the clear advantage of using a rotational NES, rather than direct proportional damping of the rectilinear motion of the vibrating cylinder is as follows. Direct proportional damping is frequently taken to be an approximate model of the dissipative motion of an imperfectly elastic spring or other restraint. It is clear that dissipation in the restraint cannot easily be used as a switch, because that would require one to turn the inelasticity on or off at will. Alternatively, one could imagine a perfectly elastic restraint, with the damping being accomplished by dissipative motion of an element connected (separately from the restraint) to the cylinder. In principle, this can be done using, say, a viscoelastic attachment, or a rigid attachment whose motion dissipates energy by means of dry friction, motion through a viscous fluid, or piezeoelectrically. But any of these approaches is mechanically more complex than the rotational NES discussed above.

V. CONCLUSION

The stability boundaries that we have computed previously [1, 2] and in §III A show that it is possible for a motionless linearly-sprung circular cylinder in cross flow at $Re < 50$ to be stabilized or destabilized by a rotational nonlinear energy sink consisting of an attached mass whose rotation about the cylinder axis is linearly damped. For combinations of Re and $1/g_n^*$ in this NES-stabilizable range (between the lower branches of the stability boundaries of the NES-less and NES-equipped cases), complete suppression of fully-developed VIV can be achieved by releasing the rotatable mass of the NES from an initially "locked" position, and cylinder vibration and vortex shedding can be turned on by locking the rotatable mass so that it has no dynamical effect on the cylinder motion and the flow. This provides a mechanism to switch on and off the effects of shedding, vibration, and unsteadiness at will.

ACKNOWLEDGMENTS

Support of this work by NSF Grant CMMI-1363231 is gratefully acknowledged.

[1] R. K. R. Tumkur, A. J. Pearlstein, A. Masud, O. V. Gendelman, A. B. Blanchard, L. A. Bergman, and A. F. Vakakis, "Effect of an internal nonlinear rotational dissipative element on vortex shedding and vortex-induced vibration of a sprung circular cylinder," Journal of Fluid Mechanics **828**, 196–235 (2017).

[2] A. B. Blanchard, L. A. Bergman, A. F. Vakakis, and A. J. Pearlstein, "Coexistence of multiple long-time solutions for two-dimensional laminar flow past a linearly sprung circular cylinder with a rotational nonlinear energy sink," Physical Review Fluids **4**, 054401 (2019).

[3] S. R. Deshmukh and D. G. Vlachos, "Novel micromixers driven by flow instabilities: Application to post-reactors," AIChE Journal **51**, 3193–3204 (2005).

[4] J. Ortega-Casanova, "On the onset of vortex shedding from 2D confined rectangular cylinders having different aspect ratios: Application to promote mixing fluids," Chemical Engineering and Processing: Process Intensification **120**, 81–92 (2017).

[5] P. F. Fischer, J. W. Lottes, and S. G. Kerkemeier, "Nek5000 web page," (2008), `http://nek5000.mcs.anl.gov`.

[6] G. B. Schubauer and H. K. Skramstad, "Laminar-boundary-layer oscillations and transition on a flat plate," NACA Report 909 (1948).

[7] H. Fasel, "Investigation of the stability of boundary layers by a finite-difference model of the Navier–Stokes equations," Journal of Fluid Mechanics **78**, 355–383 (1976).

[8] See Supplemental Material at [URL will be inserted by publisher] for supplemental movies, figures, and derivation referenced in the paper.

[9] B. J. A. Zielinska and J. E. Wesfreid, "On the spatial structure of global modes in wake flow," Physics of Fluids **7**, 1418–1424 (1995).

[10] S. W. McDonald, C. Grebogi, E. Ott, and J. A. Yorke, "Fractal basin boundaries," Physica D **17**, 125–153 (1985).

[11] Navrose and S. Mittal, "A new regime of multiple states in free vibration of a cylinder at low Re," Journal of Fluids and Structures **68**, 310–321 (2017).